Ferroelectric and piezoelectric properties of $(Bi_{1/2}Na_{1/2})TiO_3$–$BiFeO_3$ ceramics

Ichiro Fujii,[a)] Yutaka Ito, Teppei Suzuki, and Takahiro Wada
Department of Materials Chemistry, Ryukoku University, Seta, Otsu 520-2194 Japan

$(1 − x) (Bi_{1/2}Na_{1/2})TiO_3$–$xBiFeO_3$ ($x = 0$–0.9) ceramics were prepared and the ferroelectric and piezoelectric properties along with the crystal structure were investigated. The crystal system of the ceramics was rhombohedral with the $R3c$ symmetry throughout the compositions. The rhombohedral distortion ($90° − \alpha$), where α was the rhombohedral angle based on a pseudocubic perovskite cell, was minimized at $x = 0.1$, while the lattice constant increased linearly with x. Saturated ferroelectric polarization-electric field hysteresis loops were observed at $x = 0$–0.6. The coercive field was reduced at $x = 0.05$–0.2 and the high remanent polarization of 30–35 $\mu C/cm^2$ was obtained at $x = 0$–0.4. The piezoelectric constants d_{33} and $d_{33}*$ (which was calculated from a unipolar strain–electric field curve) were maximized to 93 pC/N at $x = 0.1$ and 183 pm/V at $x = 0.05$, respectively. These results suggested that the increase in the piezoelectric properties was associated with the reduction in the rhombohedral distortion, which could be useful in development of high performance lead-free piezoelectric materials.

Ichiro Fujii is an assistant professor of materials chemistry at Ryukoku University, Otsu, Japan. He received his B.S. and M.S. degrees in materials science from Tohoku University, Sendai, Japan, in 2003 and 2005, respectively. He obtained his Ph.D. degree in materials science and engineering at the Pennsylvania State University, University Park, PA, in 2010. From 2010 to 2012, he was a researcher at interdisciplinary graduate school of medical and engineering, University of Yamanashi, Kofu, Japan. In 2012, he joined Ryukoku University. His current research focuses on lead-free piezoelectric ceramics and thin films and fabrication of electrooptic transparent ceramics by pressureless sintering.

Ichiro Fujii

I. INTRODUCTION

Piezoelectric materials have been used for many applications such as sensors and actuators,[1] and recently studied for vibration energy harvesters.[2,3] For most of these applications, the piezoelectric material used is lead zirconate titanate because of the large piezoelectric properties and high Curie temperature.[4] However, lead is a toxic element and therefore lead-free piezoelectric materials have been studied.[5,6] So far, the most promising lead-free piezoelectric materials are $(K, Na)NbO_3$ and $(Bi, Na)TiO_3$–$BaTiO_3$, and proto-type devices and actual products were developed using them.[7–12] However, because of lower piezoelectric properties of both materials than those of lead

zirconate titanate, other lead-free piezoelectric materials with superior properties are desired.

Bismuth ferrite, $BiFeO_3$, is piezoelectric, rhombohedral perovskite oxide with the high Curie temperature of ~825 °C.[13] Because the synthesis of second-phase-free $BiFeO_3$ was difficult and also because a ceramic sample was so leaky and the coercive field was so large that a measurement of a well-saturated ferroelectric loop was difficult, $BiFeO_3$ ceramics were less studied until a large remanent polarization of ~60 $\mu C/cm^2$ was reported for a $BiFeO_3$ epitaxial film and a single crystal.[14,15] Intensive studies suggested that the leaky response was associated with the formation of $Bi_{25}FeO_{39}$ and the vaporization of Bi_2O_3 at high temperature and subsequent oxygen filling ($V_O^{¨} + 1/2 \, O_2 \rightarrow O_O^{×} + 2 \, h^·$) on cooling, leading to p-type conductivity,[13,16] and a large coercive field was believed to be due to Bi and O vacancies forming dipolar defect complexes, which pinned domain walls and made the ceramics ferroelectrically hard. For $BiFeO_3$ ceramics prepared from a mechanochemically activated powder to

---

minimize the Bi_2O_3 vaporization, high electrical resistivity, a saturated polarization–electric field loops with the remanent polarization of ~20 $\mu C/cm^2$, and the large electric-field-induced strain of 0.3% were reported with relatively low piezoelectric constant d_{33} values of 26–35 pC/N.[17]

One of the methods to improve the piezoelectric responses is to induce compositional phase transition by making solid-solutions with different crystal systems (ex. $PbZrO_3$–$PbTiO_3$, $(Bi_{1/2}Na_{1/2})TiO_3$–$BaTiO_3$, etc.). So far, orthorhombic $ReFeO_3$ (Re: La, Sm, and Dy),[18,19] tetragonal $BiCoO_3$,[20,21] tetragonal $Bi(Zn_{1/2}Ti_{1/2})O_3$,[22] cubic $SrTiO_3$,[23] orthorhombic $CaTiO_3$,[24] tetragonal $BaTiO_3$,[25–27] tetragonal $(Bi_{1/2}K_{1/2})TiO_3$ (Ref. 28–30) were studied as end-members for solid-solutions with rhombohedral $BiFeO_3$. In the form of thin film, increased piezoelectric responses were reported in solid-solutions with orthoferrite $SmFeO_3$ with a high-field piezoelectric constant d_{33}^* value (calculated from a strain–electric field curve) of 110 pm/V at the rhombohedral–pseudo-orthorhombic phase boundary composition of $(Bi_{0.86}Sm_{0.14})FeO_3$,[18] and solid solutions with tetragonal $BiCoO_3$ with a high-field d_{33}^* value of 100 pm/V at the rhombohedral–tetragonal phase boundary composition of $Bi(Fe_{0.9}Co_{0.1})O_3$.[21] In the form of bulk, increased piezoelectric responses were reported for solid-solutions with titanates such as tetragonal $BaTiO_3$ (Refs. 25–27) and $(Bi_{1/2}K_{1/2})TiO_3$.[28–30] For both solid-solution ceramics, the crystal system changed from rhombohedral to pseudocubic to tetragonal phases with increasing tetragonal end-member content, and the piezoelectric response was increased with keeping high Curie temperature at the composition that the crystal system changed from rhombohedral to pseudocubic phases: that is, the piezoelectric constant d_{33} of 116 pC/N and the Curie temperature of 619 °C for Mn-doped $0.75BaTiO_3$–$0.25BiFeO_3$ ceramics[26] and d_{33} of ~130 pC/N and the Curie temperature of 450 °C for $0.6(Bi_{0.5}K_{0.5})TiO_3$–$0.4BiFeO_3$ ceramics.[28,30]

Another method to increase the piezoelectric properties is to alter lattice distortion. An example is the solid-solution of $BaTiO_3$ and $(Bi_{1/2}K_{1/2})TiO_3$. The crystal system is tetragonal throughout composition, but the piezoelectric properties can be increased with decreasing tetragonal distortion (c/a) at compositions between $0.8BaTiO_3$–$0.2(Bi_{1/2}K_{1/2})TiO_3$ and $0.4BaTiO_3$–$0.6(Bi_{1/2}K_{1/2})TiO_3$.[31] The solid-solution of $BiFeO_3$ with rhombohedral $(Bi_{1/2}Na_{1/2})TiO_3$, $[(1-x)(Bi_{1/2}Na_{1/2})TiO_3$–$xBiFeO_3]$ is this type. The crystal system of the solid-solution is rhombohedral throughout composition and does not experience a compositional phase transformation at room temperature.[32,33] However, the crystal structure does change with composition; the rhombohedral distortion (90° − α) (α is measured based on a pseudocubic perovskite unit cell) is minimized at $x = 0.2$, while the lattice constant, a, is linearly increased with $BiFeO_3$ content.[32] Therefore, it is interesting to study how the dielectric, ferroelectric, and piezoelectric properties change

with the crystal structure. However, reports on ferroelectric and piezoelectric properties for the system were limited,[33–36] and a systematic study on electric properties was not reported.

In this study, $(1 - x)(Bi_{1/2}Na_{1/2})TiO_3$–$xBiFeO_3$ ($x = 0$–0.9) ceramics were prepared with solid-state synthesis, and the dielectric, ferroelectric, and piezoelectric properties along with the crystal structure and microstructure were investigated.

II. EXPERIMENTAL PROCEDURES

$(1 - x)(Bi_{1/2}Na_{1/2})TiO_3$–$xBiFeO_3$ ceramics were prepared by solid-state synthesis. Raw powders of Bi_2O_3 (99.99%; Kojundo Chemical Lab. Co., Ltd., Saitama, Japan), Na_2CO_3 (99.99%; Rare Metallic Co. Ltd., Tokyo, Japan), TiO_2 (99.9%, Kojundo Chemical Lab. Co., Ltd.), and α-Fe_2O_3 (99.9%, Kojundo Chemical Lab. Co., Ltd.) were batched according to the chemical formula with a total amount of 20 g, and they were initially mixed at 500 rpm for 20 min using a planetary ball mill (classic line P-7, Fritsch) with ethanol (20 mL) and stabilized zirconia balls with the diameter of 3 mm (40 g). After drying at 120 °C, the powders were calcined at 750 °C for 4 h in a closed alumina crucible in air. Crystal structure of the calcined powder was checked by x-ray diffraction (XRD, RINT 2500; Rigaku Corporation, Tokyo, Japan) with Cu K_α radiation. The calcined powder was milled again using the planetary ball mill with the same condition. After drying, the powder was mixed with 5 wt% polyvinyl alcohol binder and sieved through a mesh with 0.8 mm openings. Disc compacts (the diameter of 1 cm) pressed uniaxially at 200 MPa were initially heated at 700 °C for 2 h to remove the binder and then sintered at 980–1100 °C for 2 h in air.

Density was measured by an Archimedes method. Crystal structure was determined by XRD for powders crushed from sintered ceramics. Several diffraction peaks were used to determine lattice parameters by a least-square method. Lattice parameters were initially calculated on a hexagonal unit cell and then they were converted to those calculated on a pseudocubic cell (rhombohedral angle was nearly 90°) with using equations shown in literature.[37,38] The diffraction patterns were corrected by an external Si standard. For microstructural observation, a surface of the sintered ceramics was mirror-polished and then the polished ceramics were thermally etched at temperatures lower than the sintering temperatures by 100 °C for 15 min in air. The surface was observed by scanning electron microscopy (SEM, VE-9800; Keyence Corporation, Osaka, Japan). Grain size and the error bar were determined to be the average and the standard deviation of the diameters of 60–80 grains observed on an SEM image. The ceramics were
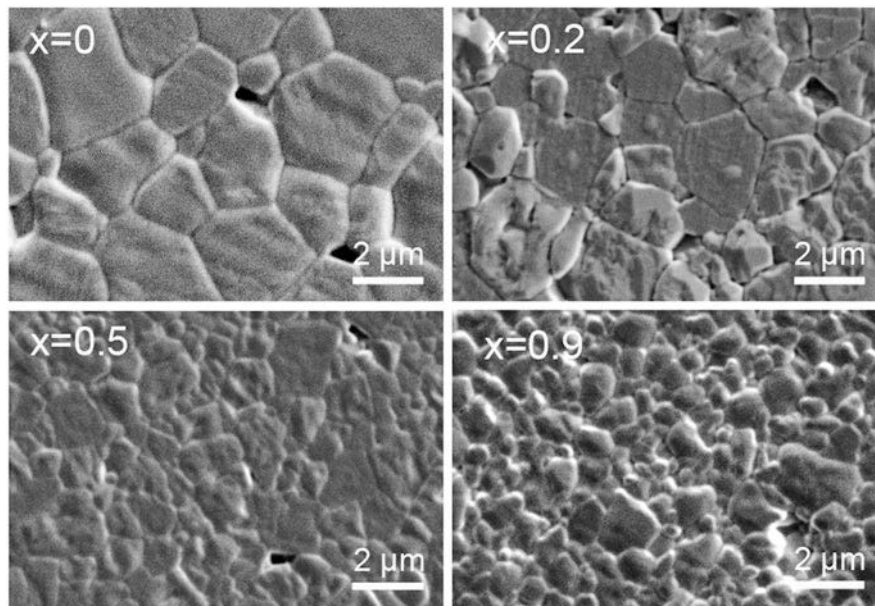
FIG. 1. SEM images of the $(1 - x)$ $(Bi_{1/2}Na_{1/2})TiO_3$–$xBiFeO_3$ (x = 0, 0.2, 0.5, and 0.9) ceramics.

TABLE I. Sintering temperature, relative density, grain size of the $(1 - x)$ $(Bi_{1/2}Na_{1/2})TiO_3$–$xBiFeO_3$ ceramics.

x	Sintering temperature (°C)	Relative density (%)	Grain size (µm)
0	1100	95	2.9 ± 0.7
0.05	1050	96	3.2 ± 1.0
0.1	1050	96	2.3 ± 0.5
0.2	1050	96	1.8 ± 0.3
0.3	1050	97	2.3 ± 0.4
0.4	1050	97	1.3 ± 0.4
0.5	980	99	1.2 ± 0.3
0.6	980	99	1.4 ± 0.4
0.7	980	98	1.3 ± 0.3
0.8	980	98	1.3 ± 0.2
0.9	980	97	1.0 ± 0.2

polished down to approximately 0.3 mm in thickness. For electrical measurements, silver paste was applied on the top and bottom surfaces of the ceramics and heated at 550 °C, and the samples were sawed to the size of $2.5 \times 2.5 \times 0.3$ mm³. The dielectric properties were determined from impedance measured at 1, 10, and 100 kHz using an impedance analyzer (4194A; Hewlett–Packard, Palo Alto, California) at temperatures from room temperature to 500 °C (on heating). Polarization–electric field (P–E) loops were measured at 0.1, 1, and 100 Hz and strain–electric field (S–E) curves were measured at 0.1 Hz using a ferroelectric tester (TF analyzer 2000; aixACCT Systems GmbH, Aachen, Germany) and a polarization and strain measuring system (Model JP005-SE; Lead Techno, Shiga, Japan) with a displacement meter (Millitron 1240; Mahr, Esslingen, Germany). The ceramic samples were poled at room temperature at 50–65 kV/cm for 5 min, and the piezoelectric constant d_{33} was measured by a d_{33} meter (Model ZJ-6B; Chinese Academy of Science, Beijing, China).
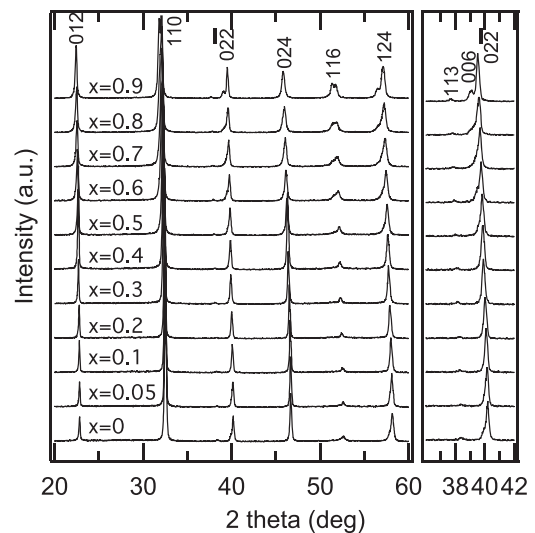
FIG. 2. XRD patterns of the $(1 - x)$ $(Bi_{1/2}Na_{1/2})TiO_3$–$xBiFeO_3$ ceramics. Diffraction peaks were indexed on the basis of the hexagonal symmetry.

III. RESULTS AND DISCUSSION

A. Microstructure and crystal structure

The microstructures of the $(1 - x)$ $(Bi_{1/2}Na_{1/2})TiO_3$–$xBiFeO_3$ ceramics were observed by SEM. As examples, the SEM images of the $(1 - x)$ $(Bi_{1/2}Na_{1/2})TiO_3$–$xBiFeO_3$ ceramics with x = 0, 0.2, 0.5, and 0.9 are shown in Fig. 1. Dense microstructures were observed. The relative density of all the ceramics prepared was 95–99%, as listed in Table I. Grain sizes were 2–3 µm at x = 0–0.3 and about 1 µm at x = 0.4–0.9 (which are also listed in Table I). The larger grain sizes for the $(Bi_{1/2}Na_{1/2})TiO_3$-rich compositions were mainly

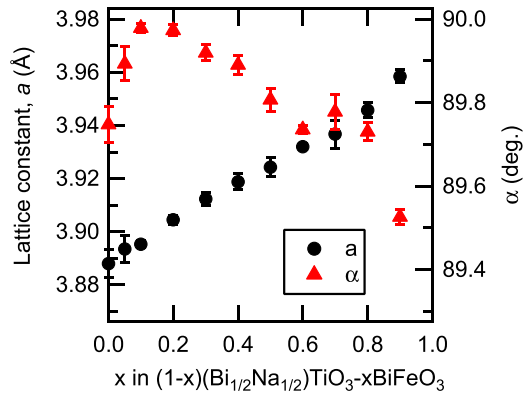FIG. 3. Lattice constant a and rhombohedral angle α for the $(1 - x)$ (Bi$_{1/2}$Na$_{1/2}$)TiO$_3$–xBiFeO$_3$ ceramics.
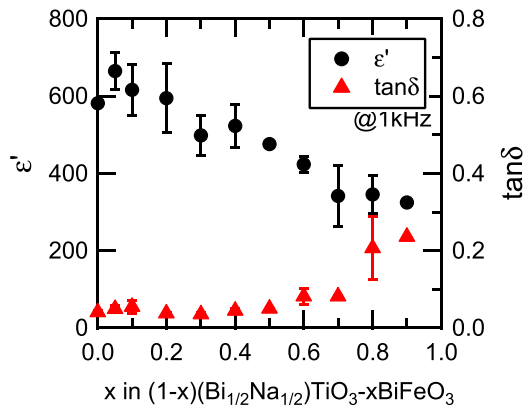
FIG. 4. Room temperature dielectric constant and loss of the $(1 - x)$ (Bi$_{1/2}$Na$_{1/2}$)TiO$_3$–xBiFeO$_3$ ceramics.

attributed to higher sintering temperatures required to densify the ceramics. Here, the melting points of (Bi$_{1/2}$Na$_{1/2}$)TiO$_3$ and BiFeO$_3$ are 1290 °C (Ref. 39) and 960–970 °C,[40] respectively.

XRD patterns of the powders crushed from the sintered ceramics of $(1 - x)$ (Bi$_{1/2}$Na$_{1/2}$)TiO$_3$–xBiFeO$_3$ (x = 0–0.9) are shown in Fig. 2. Only diffraction peaks of a perovskite phase were observed for the ceramics. The 113 diffraction peak (the diffraction peaks were indexed on the basis of the hexagonal symmetry) was observed for the perovskite phase, which meant that the samples could be assigned to the rhombohedral $R3c$ symmetry. The diffraction peaks were shifted to lower angle sides with x. Figure 3 shows the lattice constant and rhombohedral angle based on a pseudocubic cell for the $(1 - x)$ (Bi$_{1/2}$Na$_{1/2}$)TiO$_3$–xBiFeO$_3$ ceramics. The lattice constant increased linearly with x, while the rhombohedral angle showed a nonlinear behavior; it was maximized and approached to 90° at x = 0.1. Similar results were reported in literature,[32,33] except that the rhombohedral angles observed in this study at x = 0.05–0.4 was much closer to 90°, that is, 89.9–90°, compared to the α values of 89.7–89.8° at x = 0.1–0.4 from the literature. It was explained that the linear increase in the lattice constant with the BF content was mainly caused by the larger ionic radius of the Fe^{3+} ion (0.645 Å) than that of the Ti^{4+} (0.604 Å) while the ionic radii of the Na$^+$ ion (1.39 Å) and the Bi^{3+} (1.38 Å) were virtually unchanged.[32,41] On the other hand, the reason for the nonlinear behavior of the rhombohedral angle was not understood.
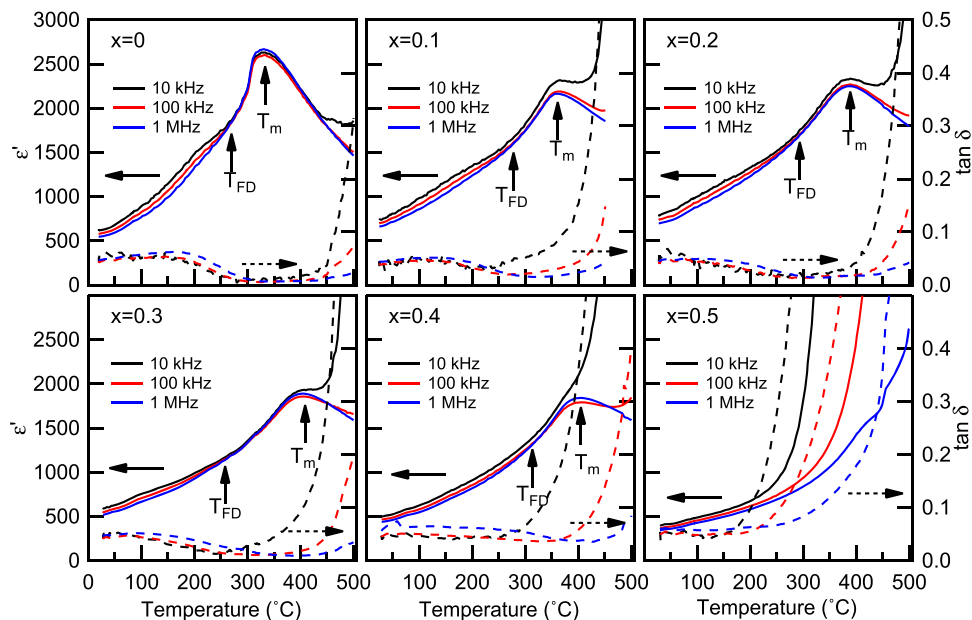

FIG. 5. Temperature dependence of the dielectric properties of the $(1 - x)$ (Bi$_{1/2}$Na$_{1/2}$)TiO$_3$–xBiFeO$_3$ ceramics. T_m is the temperature at which the dielectric constant measured at 1 MHz was maximized, and T_{FD} is the temperature at which the frequency dispersion of the dielectric constant measured at 100 kHz and 1 MHz disappeared.

B. Electric properties

The dielectric constant and loss measured at 1 kHz and room temperature for the $(1 - x)$ $(Bi_{1/2}Na_{1/2})TiO_3$–$xBiFeO_3$ ($x = 0$–0.9) ceramics are shown in Fig. 4. At $x = 0$, the dielectric constant was about 580. It increased to 600–660 at $x = 0.05$–0.2, and then decreased with x. It was speculated that the dielectric constant was increased because the samples became ferroelectrically soft owing to the reduction in the rhombohedral distortion ($90° - \alpha$). On the other hand, the decrease in the dielectric constant at $x = 0.3$–0.9 was attributed to the increase in the temperature of the dielectric maximum, T_m, with x, as shown in the next paragraph. The dielectric loss was lower than 0.1 at $x = 0$–0.7. At $x = 0.8$ and 0.9, it increased to about 0.2, which might be attributed to electric conduction.

Figure 5 shows the temperature dependence of the dielectric constant and loss of the $(1 - x)$ $(Bi_{1/2}Na_{1/2})TiO_3$–$xBiFeO_3$ ceramics ($x = 0$–0.5). At $x = 0$, two

TABLE II. T_m, T_{FD}, d_{33}*, and d_{33} of the $(1 - x)$ $(Bi_{1/2}Na_{1/2})TiO_3$–$xBiFeO_3$ ceramics. T_m is the dielectric constant maximum temperature measured at 1 MHz. T_{FD} is the temperature, at which the frequency dependence disappeared for the dielectric constant measured at 100 kHz and 1 MHz. d_{33}* is the maximum strain divided by the applied electric field for the unipolar strain–electric field curve shown in Fig. 9. d_{33} is the piezoelectric constant measured by the berlincourt d_{33} meter for poled ceramics.

x	T_m (°C)	T_{FD} (°C)	d_{33}* (pm/V)	d_{33} (pC/N)
0	331	264	131	72
0.05	336	256	182	80
0.1	360	278	140	93
0.2	389	293	153	62
0.3	404	257	110	59
0.4	403	313	88	69
0.5	...	...	32	33

anomalies were observed for the dielectric constant profile: that is, a hump around 200 °C at which the dielectric constant was frequency dependent, and the nearly frequency-independent diffused dielectric maximum peak at 331 °C. These results were consistent with previous studies.[42,43] The hump could be related to a phase transition from a ferroelectric rhombohedral phase to an antiferroelectric modulated phase, and the diffused peak could be related to an antiferroelectric orthorhombic phase to a paraelectric tetragonal phase.[44,45] Note that there is one more dielectric anomaly reported at 520–540 °C, which was not measured in this study and was associated with the tetragonal to cubic phase transition.[46] The frequency dependence of the dielectric constant measured at 100 kHz and 1MHz was disappeared at 264 °C. Here, such a temperature was defined at which the frequency dispersion disappeared by comparing dielectric constant measured at 100 kHz and 1 MHz was defined as T_{FD}. This temperature was close to the temperature that the rhombohedral phase disappeared in the modulated phase of the rhombohedral and orthorhombic phases at 280 °C.[45] With increasing x, the temperature at which the dielectric constant measured at 1 MHz was maximized, T_m, tends to increase from 331 to 404 °C at $x = 0$–0.4. At $x = 0.5$, the T_m value could not be determined due to increased conduction. On the other hand, T_{FD} was not strongly altered. The T_{FD} and T_m values are summarized in Table II. It was found that the T_m value of this study was lower than that of previous study, which might be in part associated with the smaller rhombohedral distortion ($90° - \alpha$).

Figure 6 shows the P–E loops measured at 0.1, 1, and 100 Hz for the $(1 - x)$ $(Bi_{1/2}Na_{1/2})TiO_3$–$xBiFeO_3$ ($x = 0$–0.8) ceramics. At $x = 0$, ferroelectric hysteresis loops with the remanent polarization ~30 $\mu C/cm^2$ were observed at 0.1 and 1 Hz. The remanent polarization
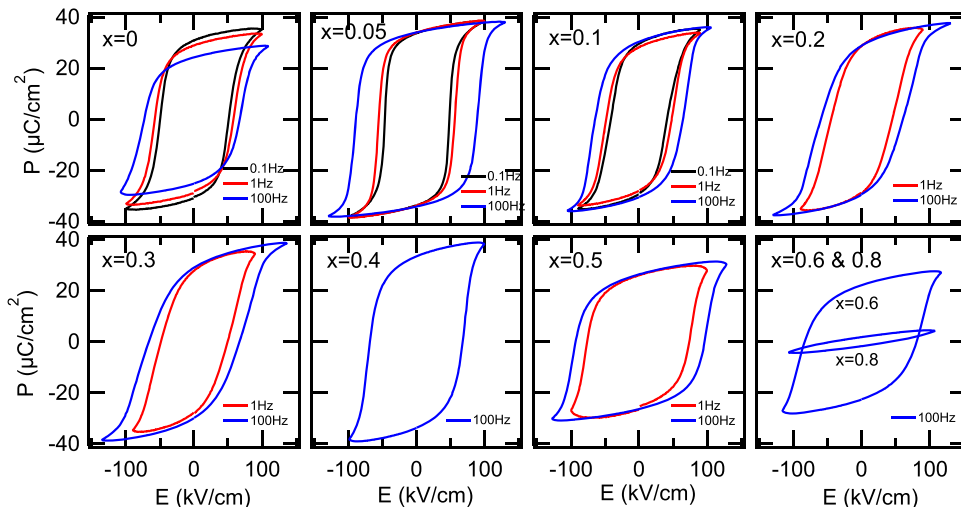

FIG. 6. P-E loops of the $(1 - x)$ $(Bi_{1/2}Na_{1/2})TiO_3$–$xBiFeO_3$ ceramics. The frequency was 0.1, 1, and 100 Hz.

measured at 1 and 100 Hz was lower than that at 0.1 Hz. This was because an electric field which was large enough to saturate the polarization could not be applied to the sample. With increasing frequency, the coercive field increased due to a slow response of domains to the electric field.[47] At $x = 0.05$–0.4, well-developed hysteresis loops with the remanent polarization of 30–35 μC/cm^2 were observed. Note that these values were much larger than those of previously reported P–E loops which were not fully saturated.[33,36] On the other hand, the coercive
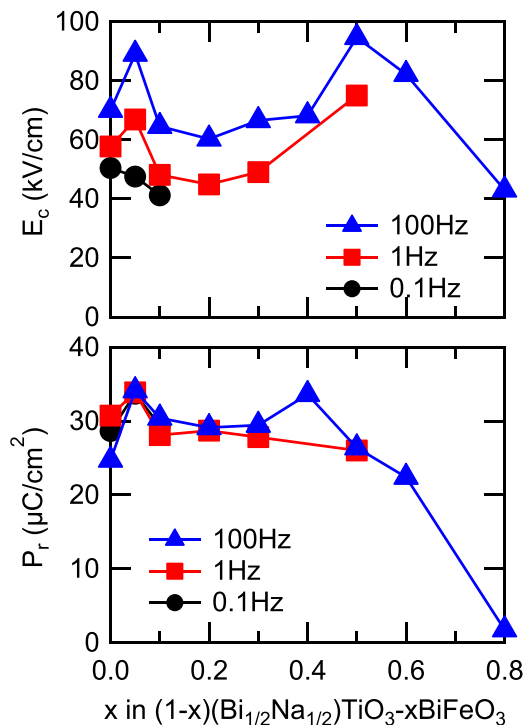
field was lowered compared to that at $x = 0$. This was attributed to the reduction of the rhombohedral distortion $(90° − α)$ which facilitated domain wall motion. At $x = 0.5$–0.8, the polarization and the opening of the ferroelectric P–E loops decreased with x, especially at $x = 0.8$. This reduction was attributed to the increased content of BiFeO$_3$ which was a hard ferroelectric material due to strongly pinned domain walls.[17] Note that the P–E loops measured at 0.1 and/or 1 Hz were not shown at $x = 0.2$–0.8 because the loops appeared leaky or the samples were electrically broken down. The remanent polarization and coercive field are summarized in Fig. 7.

The bipolar and unipolar S–E curves measured at 0.1 Hz for the $(1 − x)$ (Bi$_{1/2}$Na$_{1/2}$) TiO$_3$–xBiFeO$_3$ ceramics with $x = 0$–0.5 are shown in Figs. 8 and 9, respectively. Typical butterfly curves were observed for the bipolar measurements. At $x = 0$–0.2, the induced unipolar strain was 0.12–0.16% for the applied electric field of 80–100 kV/cm, and it was maximized at $x = 0.05$ with the d_{33}^* value (= maximum strain/applied electric field) of 182 pm/V. At $x = 0.3$–0.5, the strain was decreased with x, due to the hardening. The piezoelectric constant measured by the d_{33} meter for poled ceramics as well as the d_{33}^* value is listed in Table II. The d_{33} value of 72 pC/N at $x = 0$ was increased to 93 pC/N at $x = 0.1$, and then decreased to about 60–70 pC/N at $x = 0.2$–0.4, followed by the sudden drop to 33 pC/N at $x = 0.5$. A similar highest d_{33} value was reported by Ryu et al.,[34] but their composition dependence was different. That is, the d_{33} value was maximized at $x = 0.05$, and it dropped to about 30 and 5 pC/N at $x = 0.1$ and 0.2, respectively. The reason for the difference is unknown, but could be related to the quality of the samples or poling conditions.

In this study, it was found that the well-developed P–E loops could be obtained at $x = 0$–0.6, and the decrease in the rhombohedral distortion at $x = 0.05$–0.1 was

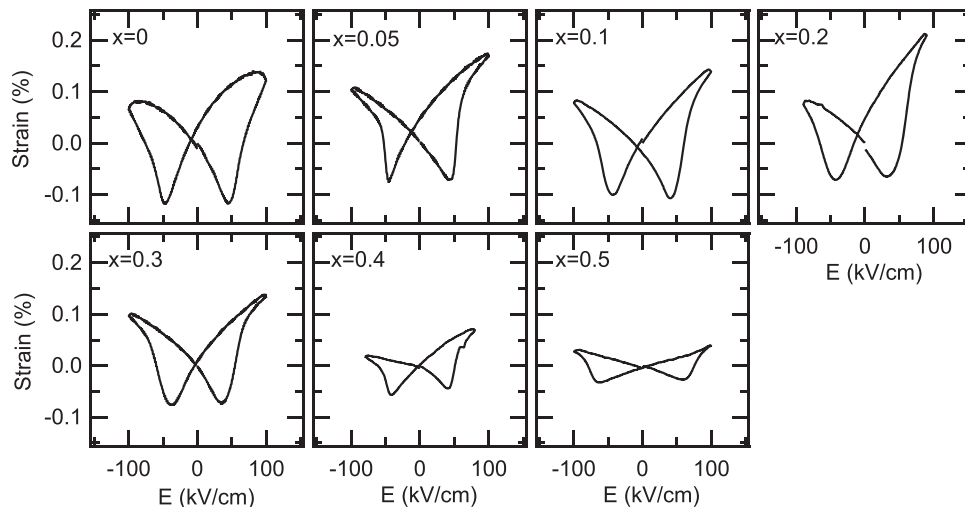FIG. 7. Remanent polarization and coercive field of the $(1 − x)$ (Bi$_{1/2}$Na$_{1/2}$)TiO$_3$–xBiFeO$_3$ ceramics.

FIG. 8. Bipolar S–E curves of the $(1 − x)$ (Bi$_{1/2}$Na$_{1/2}$)TiO$_3$–xBiFeO$_3$ ceramics. The frequency was 0.1 Hz.
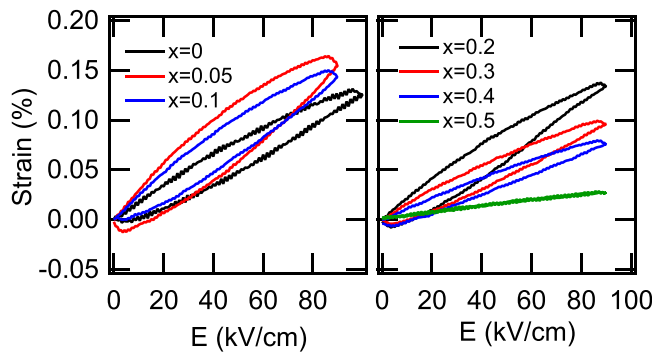
FIG. 9. Unipolar S–E curves of the $(1-x)\,(Bi_{1/2}Na_{1/2})TiO_3$–$x$$BiFeO_3$ ceramics. The frequency was 0.1 Hz.

coincident with the increased in the dielectric and piezoelectric properties while keeping T_{FD} and T_m high. These findings could be useful in development of high performance lead-free piezoelectric materials.

IV. CONCLUSIONS

The dense $(1-x)\,(Bi_{1/2}Na_{1/2})TiO_3$–$x$$BiFeO_3$ ceramics with the single perovskite phase were prepared by the solid-state synthesis. The crystal system of the ceramics was rhombohedral with the $R3c$ symmetry. The rhombohedral distortion $(90° - \alpha)$ was minimized at $x = 0.1$, while the lattice constant increased linearly with x. T_{FD} was between 256–313 °C and T_m tended to increase from 331–404 °C with x for the samples with $x = 0$–0.5, where T_{FD} is the temperature at which the frequency dispersion of the dielectric constant measured at 100 kHz and 1 MHz disappeared and T_m is the temperature at which the dielectric constant measured at 1 MHz was maximized. With increasing x, the dielectric constant increased at $x = 0.05$, and then decreased. Saturated ferroelectric P–E hysteresis and S–E butterfly responses were observed at $x = 0$–0.6 and $x = 0$–0.5, respectively. The coercive field was reduced at $x = 0.05$–0.2 and the large remanent polarization of 30–35 $\mu C/cm^2$ was obtained at $x = 0$–0.4. The piezoelectric constants d_{33} and d_{33}^* were maximized to 93 pC/N at $x = 0.1$ and 183 p.m./V at $x = 0.05$, respectively.

ACKNOWLEDGMENT

REFERENCES

1. K. Uchino: Piezoelectric actuators 2006-expansion from IT/robotics to ecological/energy applications. *J. Electroceram.* **20**(3–4), 301 (2008).
2. S. Priya: Advances in energy harvesting using low profile piezoelectric transducers. *J. Electroceram.* **19**(1), 167 (2007).
3. T. Harigai, H. Adachi, and E. Fujii: Vibration energy harvesting using highly (001)-oriented Pb(Zr, Ti)O₃ thin film. *J. Appl. Phys.* **107**(9), 096101 (2010).
4. B. Jaffe, W.R. Cook, and H.L. Jaffe: *Piezoelectric Ceramics* (Academic Press, New York, 1971).
5. T. Takenaka and H. Nagata: Current status and prospects of lead-free piezoelectric ceramics. *J. Eur. Ceram. Soc.* **25**(12), 2693 (2005).
6. T.R. Shrout and S.J. Zhang: Lead-free piezoelectric ceramics: Alternatives for PZT? *J. Electroceram.* **19**(1), 111 (2007).
7. T. Takenaka, K. Maruyama, and K. Sakata: (Bi₁/₂Na₁/₂)TiO₃-BaTiO₃ system for lead-free piezoelectric ceramics. *Jpn. J. Appl. Phys.* **30**(9B), 2236 (1991).
8. Y. Saito, H. Takao, T. Tani, T. Nonoyama, K. Takatori, T. Homma, T. Nagaya, and M. Nakamura: Lead-free piezoceramics. *Nature* **432**, 84 (2004).
9. S. Kawada, M. Kimura, Y. Higuchi, and H. Takagi: (K,Na)NbO₃-based multilayer piezoelectric ceramics with nickel inner electrodes. *Appl. Phys. Express* **2**(11), 111401 (2009).
10. T. Tou, Y. Hamaguti, Y. Maida, H. Yamamori, K. Takahashi, and Y. Terashima: Properties of (Bi₀.₅Na₀.₅)TiO₃-BaTiO₃-(Bi₀.₅Na₀.₅)(Mn₁/₃Nb₂/₃)O₃ lead-free piezoelectric ceramics and its application to ultrasonic cleaner. *Jpn. J. Appl. Phys.* **48**(7), 07GM03 (2009).
11. K. Shibata, K. Suenaga, K. Watanabe, F. Horikiri, A. Nomoto, and T. Mishima: Improvement of piezoelectric properties of (K,Na) NbO₃ films deposited by sputtering. *Jpn. J. Appl. Phys.* **50**(4), 041503 (2011).
12. T. Saito, T. Wada, H. Adachi, and I. Kanno: Pulsed laser deposition of high-quality (K,Na)NbO₃ thin films on SrTiO₃ substrate using high-density ceramic targets. *Jpn. J. Appl. Phys.* **43**(9B), 6627 (2004).
13. T. Rojac, A. Bencan, B. Malic, G. Tutuncu, J.L. Jones, J.E. Daniels, and D. Damjanovic: BiFeO₃ Ceramics: Processing, electrical, and electromechanical properties. *J. Am. Ceram. Soc.* **97**(7), 1993 (2014).
14. J. Wang, J.B. Neaton, H. Zheng, V. Nagarajan, S.B. Ogale, B. Liu, D. Viehland, V. Vaithyanathan, D.G. Schlom, U.V. Waghmare, N.A. Spaldin, K.M. Rabe, M. Wuttig, and R. Ramesh: Epitaxial BiFeO₃ multiferroic thin film heterostructures. *Science* **299**(5613), 1719 (2003).
15. D. Lebeugle, D. Colson, A. Forget, and M. Viret: Very large spontaneous electric polarization in BiFeO₃ single crystals at room temperature and its evolution under cycling fields. *Appl. Phys. Lett.* **91**(2), 022907 (2007).
16. Y. Chishima, Y. Noguchi, Y. Kitanaka, and M. Miyayama: Defect control for polarization switching in BiFeO₃ single crystals. *IEEE Trans. Ultrason. Ferroelectr. Freq. Control.* **57**(10), 2233 (2010).
17. T. Rojac, M. Kosec, B. Budic, N. Setter, and D. Damjanovic: Strong ferroelectric domain-wall pinning in BiFeO₃ ceramics. *J. Appl. Phys.* **108**(7), 074107 (2010).
18. S. Fujino, M. Murakami, V. Anbusathaiah, S.H. Lim, V. Nagarajan, C.J. Fennie, M. Wuttig, L. Salamanca-Riba, and I. Takeuchi: Combinatorial discovery of a lead-free morphotropic phase boundary in a thin-film piezoelectric perovskite. *Appl. Phys. Lett.* **92**(20), 202904 (2008).
19. D. Kan, C.J. Cheng, V. Nagarajan, and I. Takeuchi: Composition and temperature-induced structural evolution in La, Sm, and Dy substituted BiFeO₃ epitaxial thin films at morphotropic phase boundaries. *J. Appl. Phys.* **110**(1), 014106 (2011).
20. M. Azuma, S. Niitaka, N. Hayashi, K. Oka, M. Takano, H. Funakubo, and Y. Shimakawa: Rhombohedral-tetragonal phase boundary with high curie temperature in (1-x)BiCoO₃-xBiFeO₃ solid solution. *Jpn. J. Appl. Phys.* **47**(9), 7579 (2008).

21. Y. Nakamura, M. Kawai, M. Azuma, M. Kubota, M. Shimada, T. Aiba, and Y. Shimakawa: Enhanced piezoelectric constant of $(1-x)BiFeO_3$-$xBiCoO_3$ thin films grown on $LaAlO_3$ substrate. *Jpn. J. Appl. Phys.* **50**(3), 031505 (2011).

22. K. Yazawa, S. Yasui, H. Morioka, T. Yamada, H. Uchida, A. Gruverman, and H. Funakubo: Composition dependence of crystal structure and electrical properties for epitaxial films of $Bi(Zn_{1/2}Ti_{1/2})O_3$-$BiFeO_3$ solid solution system. *J. Ceram. Soc. Jpn.* **118**(1380), 659 (2010).

23. N. Itoh, T. Shimura, W. Sakamoto, and T. Yogo: Effects of $SrTiO_3$ content and Mn doping on dielectric and magnetic properties of $BiFeO_3$-$SrTiO_3$ ceramics. *J. Ceram. Soc. Jpn.* **117**(1369), 939 (2009).

24. Q.Q. Wang, Z. Wang, X.Q. Liu, and X.M. Chen: Improved structure stability and multiferroic characteristics in $CaTiO_3$-modified $BiFeO_3$ ceramics. *J. Am. Ceram. Soc.* **95**(2), 670 (2012).

25. M.M. Kumar, A. Srinivas, and S.V. Suryanarayana: Structure property relations in $BiFeO_3$/$BaTiO_3$ solid solutions. *J. Appl. Phys.* **87**(2), 855 (2000).

26. S.O. Leontsev and R.E. Eitel: Dielectric and piezoelectric properties in Mn-modified $(1-x)BiFeO_3$-$xBaTiO_3$ ceramics. *J. Am. Ceram. Soc.* **92**(12), 2957 (2009).

27. T. Futakuchi, T. Kakuda, and Y. Sakai: Multiferroic properties of $BiFeO_3$-$BaTiO_3$ based ceramics. *J. Ceram. Soc. Jpn.* **122**(1426), 464 (2014).

28. H. Matsuo, Y. Noguchi, M. Miyayama, M. Suzuki, A. Watanabe, S. Sasabe, T. Ozaki, S. Mori, S. Torii, and T. Kamiyama: Structural and piezoelectric properties of high-density $(Bi_{0.5}K_{0.5})TiO_3$–$BiFeO_3$ ceramics. *J. Appl. Phys.* **108**, 104103 (2010).

29. M.I. Morozov, M.A. Einarsrud, and T. Grande: Polarization and strain response in $Bi_{0.5}K_{0.5}TiO_3$-$BiFeO_3$ ceramics. *Appl. Phys. Lett.* **101**(25), 252904 (2012).

30. M. Hagiwara and S. Fujihara: Effects of CuO addition on electrical properties of $0.6BiFeO_3$-$0.4(Bi_{0.5}K_{0.5})TiO_3$ lead-free piezoelectric ceramics. *J. Am. Ceram. Soc.* **98**(2), 469 (2015).

31. Y. Hiruma, R. Aoyagi, H. Nagata, and T. Takenaka: Piezoelectric properties of $BaTiO_3$–$(Bi_{1/2}K_{1/2})TiO_3$ ferroelectric ceramics. *Jpn. J. Appl. Phys.* **43**, 7556 (2004).

32. V. Dorcet, P. Marchet, and G. Trolliard: Structural and dielectric studies of the $Na_{0.5}Bi_{0.5}TiO_3$-$BiFeO_3$ system. *J. Eur. Ceram. Soc.* **27**(13–15), 4371 (2007).

33. E.V. Ramana, S.V. Suryanarayana, and T.B. Sankaram: Synthesis and magnetoelectric studies on $Na_{0.5}Bi_{0.5}TiO_3$-$BiFeO_3$ solid solution ceramics. *Solid State Sci.* **12**(5), 956 (2010).

34. K.H. Ryu, T.K. Song, M.H. Kim, S.H. Lee, Y.S. Seong, S.J. Jeong, and J.S. Song: Effect of $BiFeO_3$ doping on ferroelectric and piezoelectric properties of $(Bi_{0.5}Na_{0.5})TiO_3$ and $BaTiO_3$ ceramics. *Integr. Ferroelectr.* **84**, 31 (2006).

35. A. Hieno, W. Sakamoto, M. Moriya, and T. Yogo: Synthesis of $BiFeO_3$-$Bi_{0.5}Na_{0.5}TiO_3$ thin films by chemical solution deposition and their properties. *Jpn. J. Appl. Phys.* **50**(9), 09NB04 (2011).

36. Z.M. Tian, Y.S. Zhang, S.L. Yuan, M.S. Wu, C.H. Wang, Z.Z. Ma, S.X. Huo, and H.N. Duan: Enhanced multiferroic properties and tunable magnetic behavior in multiferroic $BiFeO_3$-$Bi_{0.5}Na_{0.5}TiO_3$ solid solutions. *Mater. Sci. Eng., B* **177**(1), 74 (2012).

37. B.D. Cullity: *Elements of X-ray Diffraction*, 2nd ed. (Addison-Wesley, Reading, PA, 1978).

38. J-M. Moreau, C. Michel, R. Gerson, and W.J. James: Atomic displacement relationship to rhombohedral deformation in some perovskite-type compounds. *Acta Crystallogr., Sect. B: Struct. Crystallogr. Cryst. Chem.* **26**, 1425 (1970).

39. S.E. Park, S.J. Chung, I.T. Kim, and K.S. Hong: Nonstoichiometry and the long-range cation ordering in crystals of $(Na_{1/2}Ni_{1/2})TiO_3$. *J. Am. Ceram. Soc.* **77**(10), 2641 (1994).

40. A. Chaudhuri, S. Mitra, M. Mandal, and K. Mandal: Nano-structured bismuth ferrites synthesized by solvothermal process. *J. Alloys Compd.* **491**(1–2), 703 (2010).

41. R.D. Shannon: Revised effective ionic radii and systematic studies of interatomic distances in halides and chalcogenies. *Acta Crystallogr., Sect. A: Cryst. Phys., Diffr., Theor. Gen. Crystallogr.* **32**(5), 751 (1976).

42. V. Dorcet, P. Marchet, O. Pena, and G. Trolliard: Properties of the solid solution $(1-x)Na_{0.5}Bi_{0.5}TiO_3$-$xBiFeO_3$. *J. Magn. Magn. Mater.* **321**(11), 1762 (2009).

43. J.J. Yao, W.W. Ge, L. Luo, J.F. Li, D. Viehland, and H.S. Luo: Hierarchical domains in $Na_{1/2}Bi_{1/2}TiO_3$ single crystals: Ferroelectric phase transformations within the geometrical restrictions of a ferroelastic inheritance. *Appl. Phys. Lett.* **96**(22), 222905 (2010).

44. V. Dorcet, G. Trolliard, and P. Boullay: Reinvestigation of phase transitions in $Na_{0.5}Bi_{0.5}TiO_3$ by TEM. Part I: First order rhombohedral to orthorhombic phase transition. *Chem. Mater.* **20**(15), 5061 (2008).

45. G. Trolliard and V. Dorcet: Reinvestigation of phase transitions in $Na_{0.5}Bi_{0.5}TiO_3$ by TEM. Part II: Second order orthorhombic to tetragonal phase transition. *Chem. Mater.* **20**(15), 5074 (2008).

46. G.O. Jones and P.A. Thomas: Investigation of the structure and phase transitions in the novel A-site substituted distorted perovskite compound $Na_{0.5}Bi_{0.5}TiO_3$. *Acta Crystallogr., Sect. B* **58**, 168 (2002).

47. F. Jona and G. Shirane: *Ferroelectric Crystals* (Macmillan, New York, 1962).